ELSEVIER

Contents lists available at ScienceDirect

Additive Manufacturing

journal homepage: www.elsevier.com/locate/addma





Fast, low-energy additive manufacturing of isotropic parts via reactive extrusion

Oliver Uitz, Pratik Koirala, Mehran Tehrani, Carolyn Conner Seepersad

Walker Department of Mechanical Engineering, The University of Texas at Austin, USA

ARTICLE INFO

Keywords:
Reactive extrusion
Additive manufacturing
Low energy AM
Fast AM
Thermoset
In situ curing

ABSTRACT

Despite the well-documented advantages of additive manufacturing (AM) compared to conventional manufacturing processes, most AM technologies are subject to some significant limitations, including slow processing times, substantial energy needs, and anisotropic part properties, which become even more important as part size increases. To address these limitations, a reactive extrusion AM (REAM) process is introduced, in which successive layers of a thermoset resin are deposited and cured rapidly in situ with no external energy input aside from that required to pump and position the resin. Mechanical properties of tensile specimens fabricated in multiple orientations indicate that the tensile modulus and ultimate strength are isotropic, but elongation at break and toughness depend on orientation. The isotropic properties are attributed to chemical crosslinking of polymer chains that occurs between layers of printed parts. Moreover, the tensile modulus and strength are influenced by the local thermal environment in the build, which varies within the build envelope because of the exothermic nature of the polymerization reaction and affects the degree of curing within the specimen. The degree of curing was measured via differential scanning calorimetry (DSC) and was commensurate with the tensile strength of the tested coupons. When coupled with a large nozzle and high material flow rates, the REAM system can create nearly isotropic structural parts substantially more quickly than other AM systems, while using appreciably less energy at the point of manufacture.

1. Introduction

Reactive extrusion is an AM process in which a multi-part thermoset resin is mixed and deposited immediately by a motion-controlled extrusion nozzle to create layered structures that cure rapidly *in situ* in the ambient environment. Such a method of additive manufacturing precludes the need for time- and energy-intensive heating or illumination of the deposited material, enabling faster and more energy efficient part fabrication [1]. Unlike most direct write (DW) processes that utilize thermoset polymers [2–6], *in situ* curing in reactive extrusion eliminates the need for post-processing to achieve full strength [7,8]. *In situ* curing also facilitates chemical crosslinking of polymer chains across layers, mitigating the anisotropy observed in polymer parts created with other AM processes [1,8–13].

Although a few authors have discussed reactive extrusion in the literature over the past two decades [1,7,8,14,15], the mechanical properties of REAM parts are not well understood. Material properties for REAM parts were reported by Calvert et al. [14], but part

characterization was limited to bending tests of bar specimens with a primary raster direction along the length of the bar. Recent work from Rios et al. [7] discusses tensile strength and stiffness, but experimental characterization is limited; transverse-layer failure strain and toughness are reported for a single tensile specimen. The tensile modulus and tensile strength of transverse- and longitudinal-raster specimens are reported, as well, but more details on the number of specimens, the precise values of the properties, and the material formulations would be helpful for replicating or generalizing the results. A comprehensive analysis of mechanical properties of REAM parts as a function of orientation is lacking in the available literature and serves as a primary focus of this work.

The process most closely related to REAM—frontal polymerization—is an emerging process for additive manufacturing of thermoset parts [16]. Frontal polymerization works by mixing a resin with a latent initiator that activates and cures the resin at an elevated temperature. The exotherm associated with localized curing in turn activates the initiator in adjacent portions of the resin, creating a cascading "cure

E-mail address: ccseepersad@mail.utexas.edu (C.C. Seepersad).

^{*} Correspondence to: Walker Department of Mechanical Engineering, The University of Texas at Austin, 204 E Dean Keeton St., Stop C2200, Austin, TX 78712, USA.

front" that propagates through the material. By initializing a curing reaction and extruding the material at a flow velocity that matches the velocity of the cure front, the material effectively polymerizes as it leaves the extrusion nozzle [16]. However, the frontal polymerization process is sensitive to heat losses and restricted to only limited resin formulations, which can be costly [17].

While literature dedicated specifically to reactive extrusion and frontal polymerization is sparse [1,7,8,14–17], other methods of AM with thermoset resins are relatively well documented. Direct write is perhaps the most well documented of these processes, and can be broadly characterized by extrusion/deposition of thermoset resin that is cured post-print via conventional oven curing [2,3,6], microwave curing [4], or UV photocuring [5]. Direct write AM can produce parts that are less anisotropic than thermoplastic parts fabricated with material extrusion [2,6,9–11], but the process introduces significant limitations relative to the REAM. Because the thermoset resin is cured after the multi-layer fabrication process, as opposed to the in situ curing that occurs in a REAM system, it is more difficult to create large parts. Tall structures can slump before curing can take place, and the entire part must be placed in an appropriately sized oven, microwave, or UV curing apparatus, which contributes to processing time and makes it difficult to build large parts. For example, oven curing of parts can take more than a day [6], whereas REAM parts cure in situ. Some processes implement UV curing as the material is deposited (e.g., material jetting), but deposition rates are still much slower than those for REAM [18].

Perhaps the most ubiquitous additive technology that makes use of thermoset resins is stereolithography (SLA), in which parts are manufactured by iteratively photo-curing thin layers of resin. The size of SLA parts is limited to the dimensions of the vat in which the resin sits prior to photocuring. Analysis by Dulieu-Barton and Fulton [12] of SLA parts created with an epoxy resin typically used in stereolithography found that, much like parts created using thermoplastic additive processes, the parts are anisotropic. Although most SLA build speeds are not particularly fast, recent work from de Beer et al. [19] has achieved significant improvements in SLA build speeds, achieving vertical build rates as large as 2 m per hour, representing an increase by two orders of magnitude relative to typical SLA machines. These systems provide an aspirational build rate benchmark for reactive extrusion systems.

An alternative to direct write AM of thermosets—the DART (Diels-Alder reversible thermoset) process—leverages dynamic covalent chemistry to print with thermosets in a process similar to thermoplastic extrusion [20]. The unique chemistry of the stock material facilitates de-crosslinking and melt processing at elevated temperatures and re-crosslinking at lower temperatures. Resulting parts exhibit low degrees of anisotropy [20], but commercial availability of Diels-Alder thermoset formulations is limited with most of them synthesized in-lab by researchers themselves. In contrast, reactive extrusion systems can accommodate a wide variety of commercially available two-part thermoset formulations with relatively short gel times.

Although fused filament fabrication (FFF) systems use thermoplastic feedstocks, they are similar to reactive extrusion systems insofar as they both deposit flowable polymer that solidifies *in situ*. Parts produced by FFF systems are notoriously anisotropic with transverse-layer strengths as low as 15% that of longitudinal-raster strengths, which, in turn, are appreciably weaker than the strength of the bulk material [10,11,21]. Researchers have reduced the anisotropy of FFF parts using a number of novel techniques [22,23], though such techniques require additional energy input and material processing that is not needed in a REAM system.

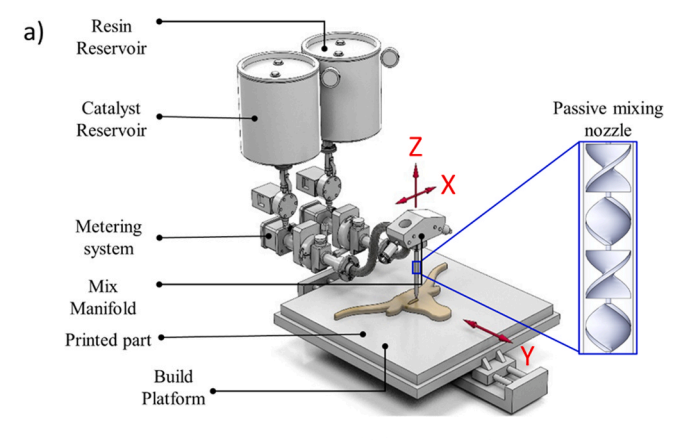
In spite of its promise, REAM remains an underexplored topic. Relative to other thermoset AM technologies, the literature on REAM is sparse, and the existing literature does not provide comprehensive coverage of the mechanical properties of resulting parts and system functionality relative to other competing AM processes. This paper focuses primarily on investigating the orientation-dependent mechanical properties of REAM parts in the context of their exothermic curing

process. Accordingly, this paper is the first to report statistically analyzed, orientation-dependent mechanical properties of REAM parts. These results are accompanied by a full description of all aspects of the REAM system, including all relevant mechanical components, the feedstock material formulation, and the process parameters. Additionally, the effects of exothermic curing kinetics on the properties of REAM resin/catalyst mixtures and parts are evaluated and characterized.

2. Overview of the reactive extrusion AM system

A generalized schematic of the reactive extrusion AM system is presented in Fig. 1. The metering system draws two precursors—thermoset resin and hardening (catalyst) agent—from separate reservoirs and pumps them in a precise ratio into the mix manifold. The separate streams of resin and hardener join as they exit the mix manifold and enter the mixing nozzle. The mixing nozzle passively mixes the precursors together, triggering a polymerization process that completes after the material is deposited. The mix manifold and mixing nozzle are mounted to a positioning system—either a gantry system or a robotic arm—which is synchronized with the metering system to deposit material in the appropriate locations.

To support iterative process refinement and small-batch experimentation, the general schematic in Fig. 1 is embodied as a desktop system, which pairs the metering system with an off-the-shelf FFF printer. Precursors are stored in separate 8 L stainless steel reservoirs. The metering system consists of a twin-piston positive displacement pump driven by a stepper motor linear actuator (NEMA 34, 3.12 A, 5 V, 1000 N, non-captive with 2.54 mm travel/revolution). The precursors enter the mix manifold (Glenmarc) in separate channels and exit into a mixing nozzle (Sulzer Mixpac MS 10–18 T, 214 mm long, 10 mm inner diameter). The nozzle contains an internal geometry that induces turbulent flow in the precursors and produces a more homogeneous mixture at the nozzle exit. The desktop FFF printer, a Lulzbot Taz 6, accommodates the new system by replacing the original print head on



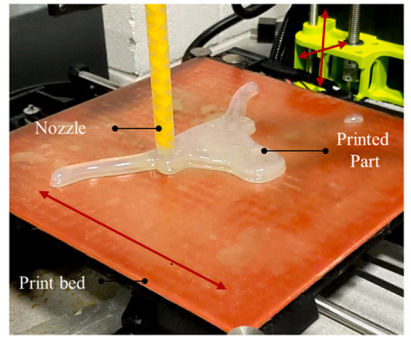


Fig. 1. (a) Generalized schematic of a REAM system: a metering system pumps thermosetting precursors together through a position-controlled mixing nozzle. (b) University of Texas longhorn logo printed on the REAM system testbed.

b)

the gantry carriage with the mix manifold and nozzle.

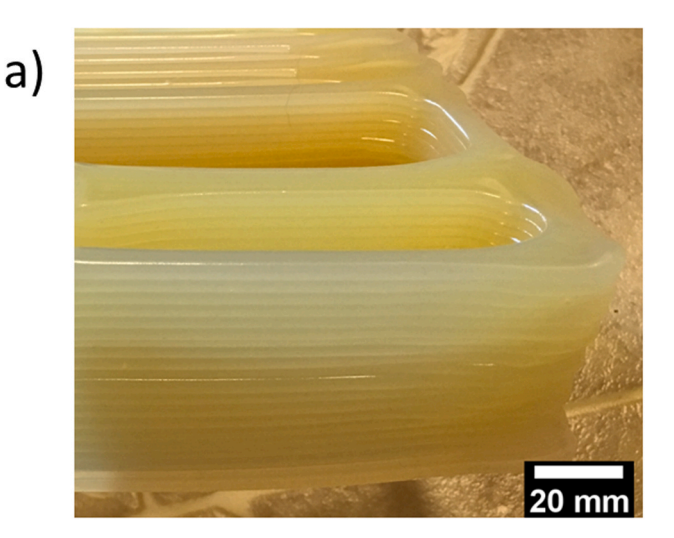
Path planning is performed using Cura (v4.0, Ultimaker, LGPLv3 license), an open source software application that slices parts into layers and generates G-code instructions for building each layer. The geometric properties of the system—nozzle length, nozzle exit diameter, and build volume dimensions—are specified within Cura to generate appropriate deposition paths and material flowrates. To synchronize the motion of the gantry carriage and the metering system, signals that typically drive the filament extrusion motor are redirected to the stepper motor that drives the piston pumps in the metering system. The G-code generated by Cura is post-processed to include commands that prime the nozzle prior to printing and halt movement of the gantry system and reset the piston pumps as needed.

Parts are fabricated from EPON 8111 epoxy resin (Hexion Inc.®) mixed with EPIKURE 3271 curing agent (Hexion Inc.®) with a 4:1 ratio by volume. This material was selected for its mechanical properties, rapid gel time, and low viscosity. Its published tensile and flexural strengths of 69.0 and 108 MPa [24], respectively, are similar to those of construction grade lumber and support structural applications [25]. A rapid gel time of 1 min for EPON 8111 combined with EPIKURE 3271 [26] helps it support subsequent layers during the printing process without slumping. EPON 8111's viscosity of 800–1100 cP at room temperature is too low to hold its shape after printing, but the viscosity and storage modulus are increased by adding a thickening agent, fumed silica (E K Industries Inc.®, CAS No. 112945-52-5), at 3.5% by weight.

The weight percentage of fumed silica was tuned via experimentation to identify a composition that supported buildability; specifically, the ability to print multiple layers without flowing, collapsing, or sagging after deposition. Resin and hardener sample volumes of 24 mL and 6 mL, respectively, were mixed with varying weight percentage concentrations of fumed silica and qualitatively tested for their ability to retain their shape after deposition. Six resin/hardener samples with weight percentages of fumed silica ranging from 0% to 9% by weight were mixed for 20 s and poured onto a polyimide film, and their shapes were documented (Fig. 2). Samples with weight concentrations of fumed silica less than 2.5% were found to be incapable of retaining vertical edges. Formulations with 2.5% and 3.5% fumed silica by weight retained vertical edges and samples with 5% or more were capable of retaining overhangs.

Based on these results, a trial print was conducted with 3.5% fumed silica by weight. Fumed silica was mixed with the resin using a power drill driven spiral mixing paddle, and the mixture was degassed by allowing it to settle at room temperature and pressure for 7 days. Mixtures with higher contents of fumed silica would have required a vacuum and heat (to lower the viscosity) for degassing. Resulting parts maintained geometric fidelity during the deposition process. As shown in Fig. 3a, walls with widths of 6 mm and heights of 48 mm proved to be manufacturable with this formulation.

Resin samples with varying weight percentage concentrations of fumed silica were subjected to rheological tests at room temperature immediately after mixing. A rheometer (TA Instruments, Discovery



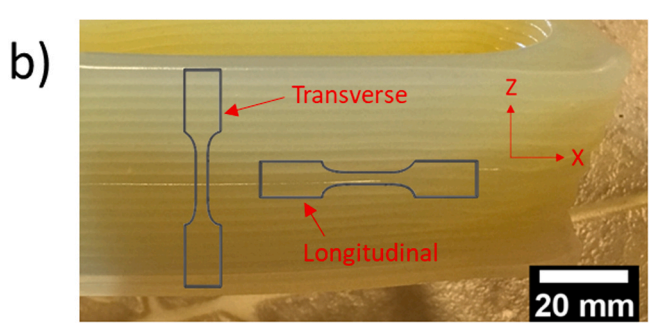


Fig. 3. (a) REAM test part made with a 3.5 wt% fumed silica material formulation (raster width \sim 6 mm, raster height \sim 2.4 mm, 20 layers). (b) REAM test part with overlayed coordinate system and tensile bars.

DHR-2) with 40 mm parallel plate geometry and a constant gap of 500 µm was used for the rheological characterization. A continuous flow sweep was performed at controlled shear rates from 0.01 to 100 s⁻¹ at room temperature to observe the effect of shear rate on viscosity. As shown in Fig. 4, the addition of fumed silica increased the viscosity of the resin significantly by up to three orders of magnitude. The static viscosity of a printable formulation of 3.5 wt% fumed silica, measured at a shear rate of $\sim 0.01 \text{ s}^{-1}$, was found to be 4.7 Pa s and to decrease to 2.4 Pa s at a shear rate of 100 s⁻¹. Moreover, shear thinning was observed for all fumed silica specimens but was more pronounced for highly loaded samples. The static viscosities of the 7.5 wt% and 9 wt% silica filled resins were found to be on the order of 10^2 and 10^4 , respectively, and to decrease to \sim 6 Pa s at shear rates > 100 s⁻¹. It has been shown that larger weight percentages of fumed silica or other fillers could be utilized without sacrificing pump-ability by leveraging the shear thinning effect observed in these tests and increasing the

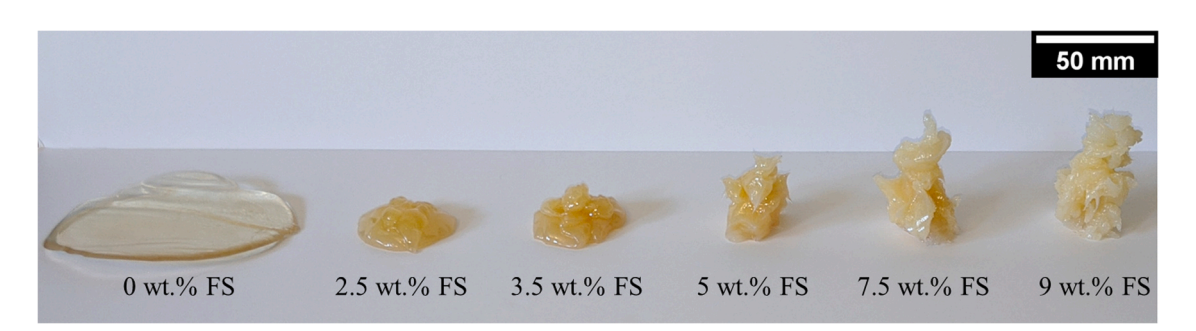


Fig. 2. Resin/hardener samples with various weight percentage concentrations of fumed silica (from left to right: 0%, 2.5%, 3.5%, 5%, 7.5%, 9%), mixed and poured/scooped onto substrate.

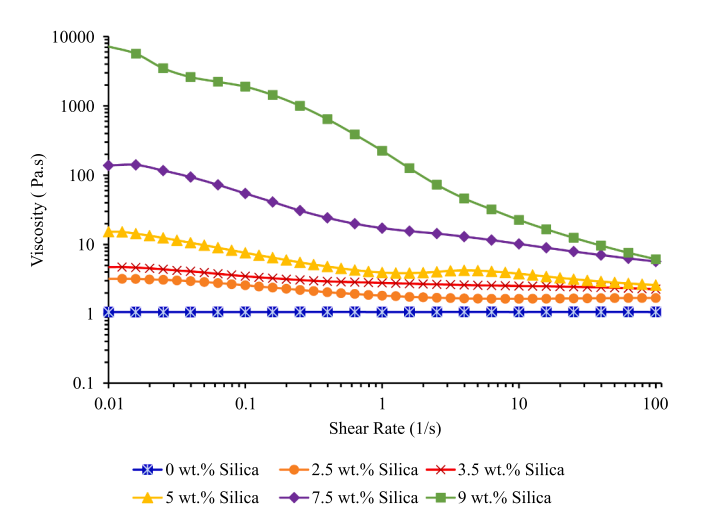


Fig. 4. Shear-rate-dependent viscosity of EPON 8111 resin filled with fumed silica.

temperature of the precursors to reduce the viscosity [27].

The rheological behavior of the resin/catalyst mixture immediately after mixing was examined by measuring the flow behavior of the mixture. Specifically, a 100 mL syringe with a 7.5 mm diameter nozzle was filled with freshly hand-mixed resin/catalyst mixture (without fumed silica) and immediately mounted on an Instron® 3345 load frame equipped with a 5 kN load cell and compression platens. The testing instrument then depressed the syringe plunger at a constant rate of 2 mm/s and recorded the force exerted on the syringe plunger as a function of time. Using this data, as well as videos of the syringe extruding the resin/catalyst mixture, the cure kinetics related to gelation were characterized.

A pressure vs. time plot for one such test is illustrated in Fig. 5. In the trial, an initial spike in pressure occurs as the compression platen comes into contact with the plunger, overcoming static friction between the plunger and syringe to initiate plunger motion and material flow. The material exhibits a low, relatively constant viscosity until approximately 1 min after the resin and catalyst are mixed. Then, the material begins to gel and its viscosity increases steadily, requiring the compression platen to exert more force on the plunger to maintain a constant 2 mm/s displacement rate. A subsequent, more dramatic rise in pressure occurs at approximately 70 s post-mixing. Video evidence suggests this rise in pressure is a result of irregular flow behavior as the material gels and increases in viscosity; the material begins "sputtering" from the nozzle at approximately 76 s. This sputtering behavior eventually gives way to intermittent extrusion of rubbery, semi-cured epoxy. By 80 s, the material leaving the nozzle is clearly viscoelastic in nature and no longer flows smoothly. The sharp peaks and valleys beyond the 80 s mark are likely caused by a small amount of air in the syringe. In practical terms, the behavior of the material beyond the apparent gel time of approximately 60–76 s is irrelevant because it no longer flows well enough to generate repeatable deposition patterns in the REAM system.

Supplementary material related to this article can be found online at doi:10.1016/j.addma.2021.101919.

The primary implications of this test are two-fold. First, material should not be kept in the static mixing nozzle for longer than 1 min in order to ensure the material at the end of the nozzle does not gel and negatively impact the deposition pattern. Second, assuming the material cannot support additional layers prior to gelation, the time interval between deposition of subsequent part layers should be at least 1 min.

The material formulation used in this study is similar to those recommended by Rios et al. [28], consisting of an amine component, an isocyanate component, thickened with either precipitated or fumed silica. They found that printable materials exhibit a shear storage modulus greater than 2000 Pa and a ratio of shear loss modulus to shear storage modulus less than 1.5 prior to curing [7]. Furthermore, they found that the shear storage and shear loss moduli must be greater than 1,000,000 Pa and 600,000 Pa, respectively, 6 min after deposition.

3. Specimen fabrication and testing

The process parameters for REAM are adjustable for targeting different deposition rates and levels of geometric fidelity. For the sake of consistency and repeatability, however, a set of standard process parameter values was adopted for the parts described in this paper. As shown in Table 1, the values include a relatively large nozzle diameter, layer height, and material flow rate compared to most desktop material extrusion systems. The material flow rate of 102 mL/min, for example, is 50 times larger than a recently developed high speed desktop FFF system and 350 times larger than standard desktop FFF systems [29]. This combination of extrusion rate and nozzle diameter produces adequate mixing of the thermoset precursors in the mixing nozzle without exceeding the print speed capabilities of the desktop gantry system or compromising the geometric fidelity of the parts. Since the polymerization reaction is exothermic, the parts are subject to steep temperature gradients and associated warping and curling. To mitigate these effects,

 Table 1

 Process parameter values employed in this study.

Process variables	Value	Units
Nozzle diameter	6.5	mm
Nozzle length	214	mm
Print speed	0.11	m/s
Material flow rate	102	mL/min
Layer height	2.5	mm
Build plate temperature	60	°C
Material gel time	~1	min

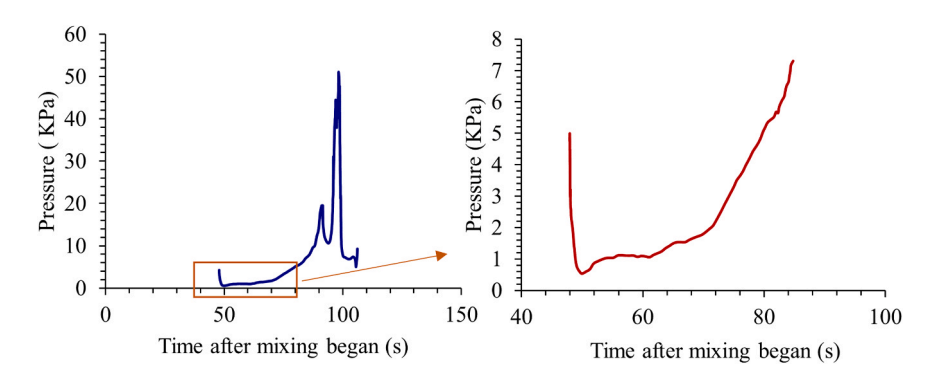


Fig. 5. Pressure versus time for syringe study of the flow behavior of the resin/catalyst mixture immediately after mixing (left) with a magnified view of the first 85 s (right).

the build plate temperature is set to $60\,^{\circ}\text{C}$, and the parts are built directly on the build plate after applying a thin film of mold release agent. Fabricating initial test parts on polyimide tape led to warping and failed builds because the tape detached from the build plate during fabrication.

The exothermic nature of the polymerization reaction necessitates a cool-down period before the part can be removed from the build plate. To investigate the extent of the temperature increase, a cubic sample part with bounding dimensions of approximately 2.5 cm was fabricated, and its surface temperature was monitored with an IR camera (FLIR T420 thermal imaging, 76,800 pixels and 7.5–13 μm spectral range) during and after deposition. Thermal imaging revealed that the part

temperature starts to rise after 1 min (Fig. 6a) and peaks at approximately 200 °C after approximately 4 min. Significant thermal gradients were observed after the material had been allowed to cure under ambient conditions for 13 min (Fig. 6). These thermal effects required a cool-down period of approximately 30 min for the part in Fig. 6, at which point the part was cool enough to be removed from the build plate by hand. Thermal gradients from the exterior to the interior of the part were witnessed throughout the curing and cooling periods. The peak temperatures and thermal gradients could be minimized by reducing part density (e.g., less part infill and smaller solid sections within parts). The positive side effects of minimizing thermal gradients could include reduced residual stresses and reduced tendency to warp during the build

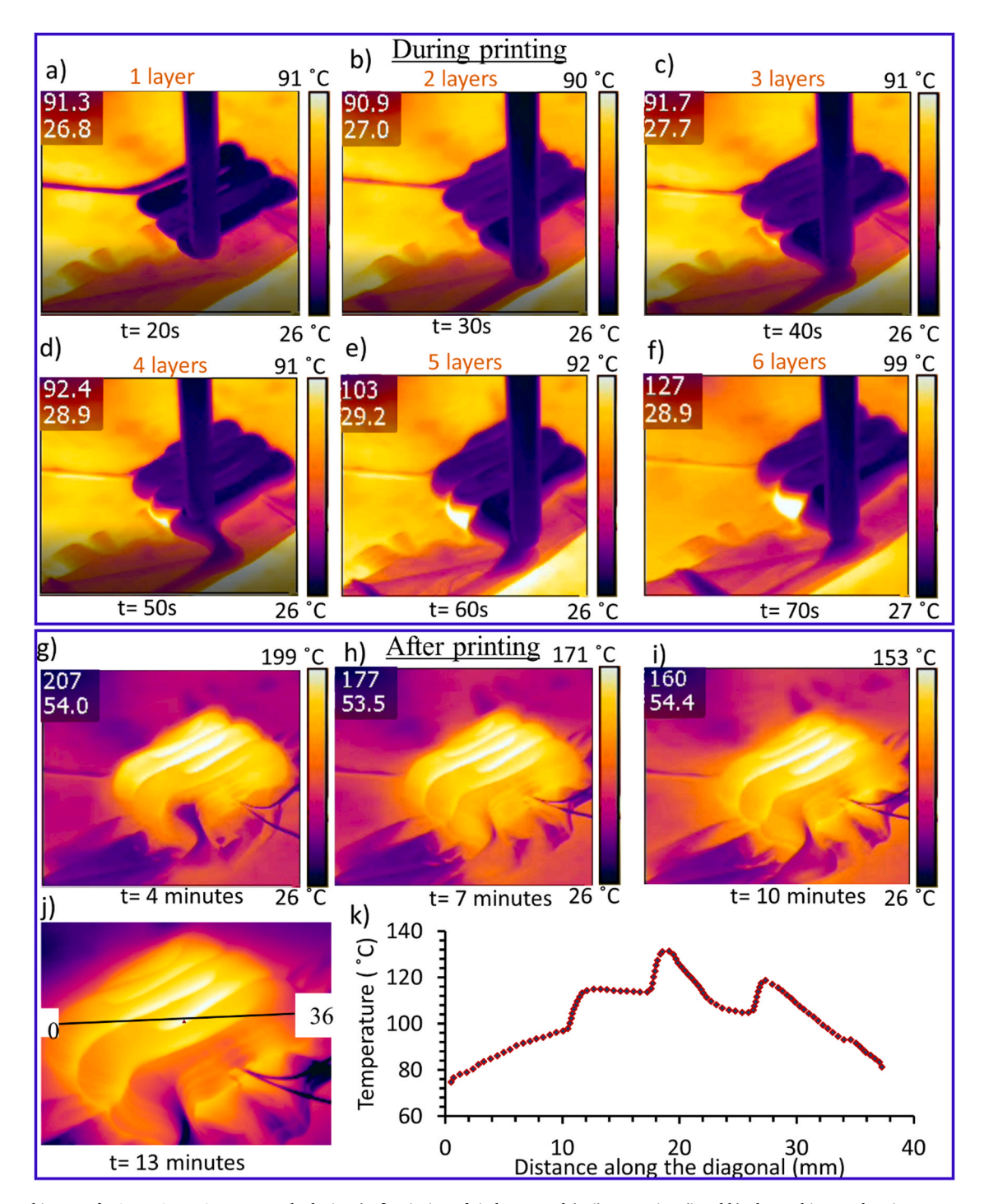


Fig. 6. Thermal image of a $2.5 \times 2.5 \times 2.5$ cm sample during (a–f) printing of six layers and (g–i) post-print. (j and k) Thermal image showing temperature gradient along the diagonal of the partially cooled specimen after 13 min.

process. Further work must be conducted to quantify these effects in a meaningful way.

Prior to fabricating parts for mechanical testing, a variety of sample parts were fabricated to refine the processing parameters. The sample part in Fig. 7 illustrates the REAM system's ability to fabricate parts with reasonable geometric fidelity. As shown, the part is 230 mm wide, 95 mm from the end of the snout to the top of the head, and 16 mm thick, consisting of 4 layers of material. The part was fabricated in less than 3 min after priming the nozzle. A small break in the infill pattern is noticeable near the bottom of the part, which was caused by momentary backlash in the metering system.

After identifying the process parameter settings in Table 1, parts were fabricated for mechanical property testing. The strategy was to print bulk parts from which tensile specimens could be machined. As shown in Figs. S1 and 3b, a series of thin vertical walls were fabricated. The horizontal dimension of the walls was oriented along the X direction of the printer, and the vertical along the Z (Fig. 1a). Each of the six walls was a single raster wide (6.5 millimeters), 70 millimeters tall, and 115 millimeters long. The material cured for 2 weeks at room temperature, complying with the cure schedule prescribed for EPON 8111. Subsequently, 29 tensile specimens conforming to ASTM D638 Type V were cut from the walls and surfaced via CNC milling machine. Care was taken to cut the specimens such that their gauge length contained no gaseous inclusions, which are visible in Fig. S1 and most likely caused by air bubbles entrapped between the layers. Longitudinal and transverse specimens were cut such that their gauge lengths were either parallel or perpendicular to the rasters that constituted the walls (Figs. 3b, S1). These two orientations were chosen so that both the longitudinal- and transverse-layer strength of parts created with the REAM system could be evaluated.

As shown in Fig. 8, the color of the specimens varied significantly. Color was hypothesized to be a visible indication of the extent of curing since darker specimens were extracted primarily from the interior of the build where peak temperatures were higher; this hypothesis is proved later by the direct measurements of the degree of curing (DoC) for these samples. Accordingly, the specimens were grouped visually into three categories according to color: white, yellow, and orange. The relationship between color, degree of cure, and tensile strength is investigated in the results section. The specimen labeled "1" appears much darker than other specimens; its darkness is an artifact of ink stains from using it as a stencil to trace the profiles of other specimens. Differential Scanning Calorimetry (DSC) was utilized to measure the DoC of the differently colored specimens. A DSC 214 Polyma from Netzsch was used for this characterization. Each scan was performed in an inert atmosphere; under a 40 mL/min nitrogen gas flow. Two samples, each weighing 5-10 mg, were tested from each color category. The test was performed from room temperature to 350 °C at a heating rate of 10 °C/min.



Fig. 7. Longhorn created in 3 min via reactive extrusion additive manufacturing. The part is 230 mm from horn tip to horn tip, 95 mm from the top of the head to the end of the snout, and 16 mm thick.

Proteus® 80 DSC software was used for the analysis of heat flow and enthalpy calculation. Residual enthalpy of post-curing, H_{pc} , for partially cured (REAM prepared) specimen and reaction enthalpy (enthalpy of complete curing), H_r , was determined by integrating the exothermic peaks. Mixed resin and catalyst was also tested in DSC instantly after mixing to measure the reaction enthalpy (H_r). The degree of cure (α) was then calculated using the following relation:

$$\alpha(\%) = (1 - \frac{\Delta H_{pc}}{\Delta H_c}) * 100 \tag{1}$$

Tensile testing was performed using an Instron® 3345 load frame for the collection of load data and an internally developed digital image correlation (DIC) system [30] for the collection of strain data. A Basler® Ace camera (model number acA3088-16gm) and an Edmund Optics® lens (model number 67-709) constitute the optical hardware of the DIC system, with a pair of gooseneck LEDS diffused with nylon fabric providing appropriate lighting. All optical hardware was rigidly attached to the load frame using an adjustable mounting frame.

In preparation for testing with the DIC system, all tensile specimens were painted white and speckled with a thin coat of black paint on one side. The highly visible speckle patterns were trackable by DIC software using a series of high-resolution images taken during testing. The speckled tensile specimens were individually loaded into the grips of the load frame, pre-strained, and quasi-statically loaded at an extension rate of 1 mm/min. Concurrently, images of each specimen's gauge length were recorded and stored using the Basler® pylon software package. Virtual extensometer strain measurements of the captured images were performed using Digital Image Correlation Engine (DICe), a software package developed by Sandia National Labs for the purposes of image analysis. DICe analysis of specimen images prior to loading suggests a strain noise floor of 0.000168 or 0.0168% strain. The time domains associated with the load and strain data were synchronized using custom python software by identifying and pairing the discontinuities associated with specimen fracture.

4. Results and discussion

The quasi-static stress-strain responses of the tensile specimens were used to evaluate the tensile modulus, elongation at break, toughness, and ultimate strength. Plots of engineering stress versus engineering strain for all specimens are overlaid in Fig. 9, where red and blue plots represent longitudinal and transverse specimens, respectively. Visual inspection of these plots indicates noticeable variation in the tensile modulus and strength of the specimens. Although the orientation dependency of part strength is not clear, given the premature failure of specimens in both categories, the specimens with the greatest elongation at break are exclusively longitudinal specimens, indicating that orientation appears to be having an effect on mechanical properties.

Fig. 10 contains plots of the tensile modulus for all tested specimens separated by layer orientation. The mean and standard deviation of the data for all specimens are 3.51 GPa and 0.62 GPa, respectively. Although the tensile modulus of EPON 8111 is not published by Hexion®, the flexural modulus is published at a value of 3.45 GPa, which differs from the experimental mean tensile modulus by less than 2%. A t-test supports the null hypothesis that there is no statistically significant difference (p = 0.57) between the published and experimentally determined values; however, appreciable spread exists in the experimental tensile modulus data, which is apparent in Figs. 9 and 10.

The mean values of tensile modulus for the transverse and longitudinal specimens were very similar at 3.69 and 3.32 GPa, respectively. The standard deviation for the transverse specimens (0.69 GPa) was larger than that of the longitudinal specimens (0.48 GPa) and the aggregated specimens, indicating that the variability in the aggregated analysis is unlikely to be attributable to orientation effects. A t-test (p = 0.106) supports the null hypothesis that there is no statistically significant difference in tensile modulus between the two orientations;

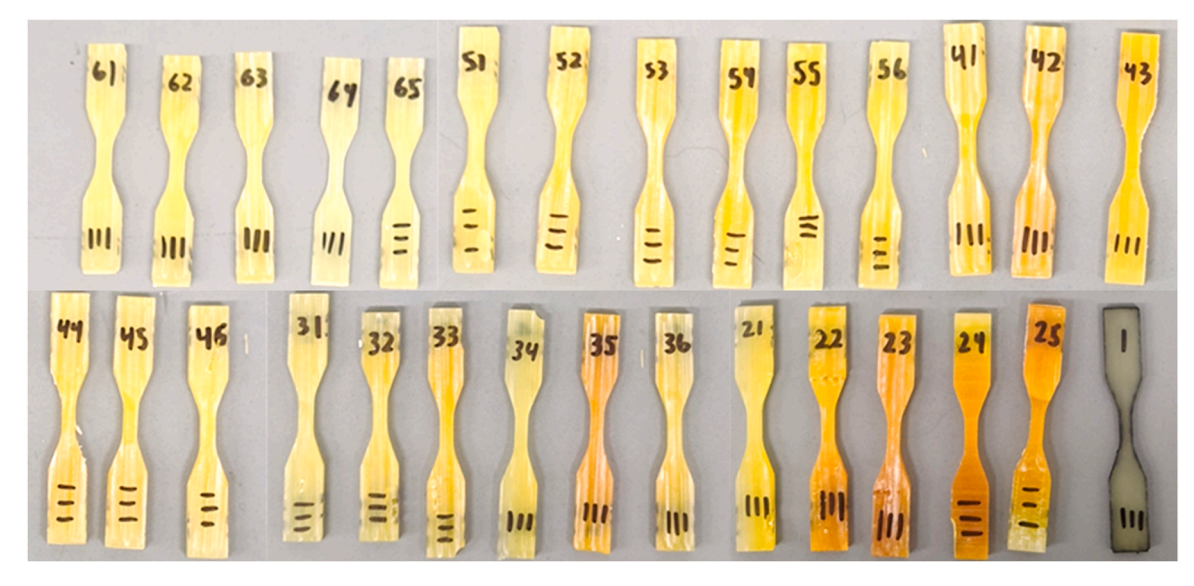


Fig. 8. Photo of all tested tensile specimens illustrating the variation in color (degree of cure). (For interpretation of the references to color in this figure legend, the reader is referred to the web version of this article.)

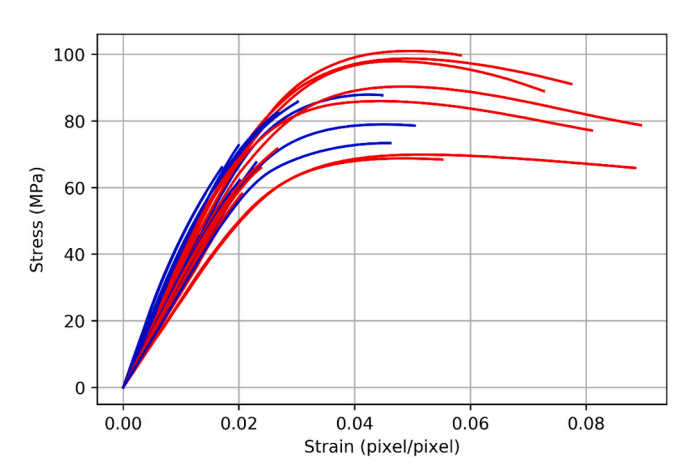


Fig. 9. Plots of engineering stress versus engineering strain for all 29 tensile specimens with transverse specimens plotted in blue and longitudinal specimens plotted in red. (For interpretation of the references to color in this figure legend, the reader is referred to the web version of this article.).

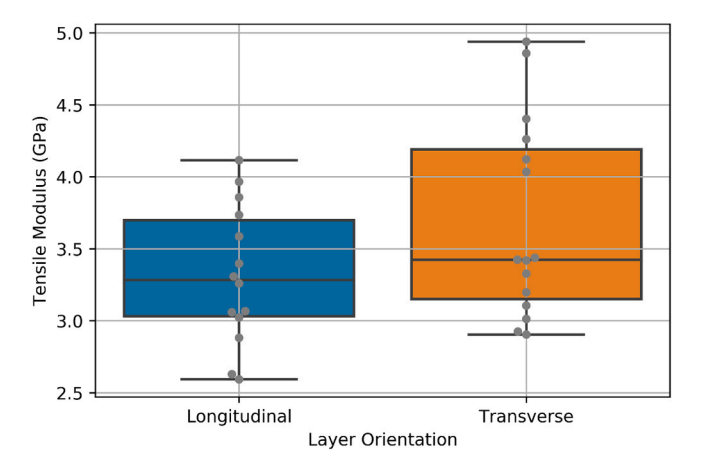


Fig. 10. Tensile modulus of all specimens separated by layer orientation.

the t-test was preceded by a normality test and a Levene test with p-values of 0.231 and 0.299, respectively, leading to acceptance of the null hypotheses that the data sets were normally distributed and of equal variance. Categorizing the tensile specimens according to color (and therefore, degree of cure) also failed to identify any statistically significant differences in tensile modulus. Overall, despite the variation observed in the tensile modulus, the mean values are consistent with the published flexural modulus value of 3.45 GPa.

The specimens also exhibited some interesting failure behavior. Ultimate tensile strength is identified as the maximum stress endured by the part prior to failure, values for which are plotted in Fig. 11. The mean ultimate tensile strength of all specimens is 71.3 ± 15.3 MPa. A comparison with the published value of 69.0 MPa supports the null hypothesis that there is no statistically significant difference from the published value (t-test, p = 0.41). Close observation of Fig. 9 reveals that some specimens exhibit ductile failure with necking and relatively large strains prior to fracture, whereas others exhibit brittle failure with almost no plastic deformation prior to fracture. Fig. 11 shows the tensile strengths of the ductile and brittle failure specimens clustering together, which motivates a comparative analysis. The mean tensile strengths of the ductile and brittle specimens are 85.3 \pm 12.1 and 64.0 \pm 11.2 MPa, respectively. T-tests reject the null hypotheses that there is no statistically significant difference between the ductile and brittle ultimate tensile strengths (p = 0.000063) or between the ductile ultimate tensile strength and the published value (p = 0.0021), but a *t*-test supports the null hypothesis that there is no statistically significant difference between the brittle ultimate tensile strength and the published value (p = 0.071). Overall, the brittle specimens exhibit ultimate tensile strengths that correspond closely to published values for this material, while the ductile specimens are significantly stronger.

Fig. 11 reveals that more transverse specimens experienced brittle fracture and that their ultimate strengths varied more than those of the longitudinal specimens. These results suggest that transverse bonding could be a factor in brittle failure. The mean tensile strengths of the brittle-longitudinal and brittle-transverse specimens are 63.6 ± 6.7 and 64.2 ± 13.5 MPa, respectively. A t-test indicated no statistically significant difference between brittle transverse and longitudinal specimen tensile strengths (p = 0.91). Fig. 11 also shows greater variability in the longitudinal tensile strength than the transverse strength for ductile specimens, a reversal of the phenomenon observed for brittle specimens. The mean tensile strengths of the ductile-longitudinal and ductile-transverse specimens are 87.5 ± 13.5 and 80.1 ± 7.3 MPa,

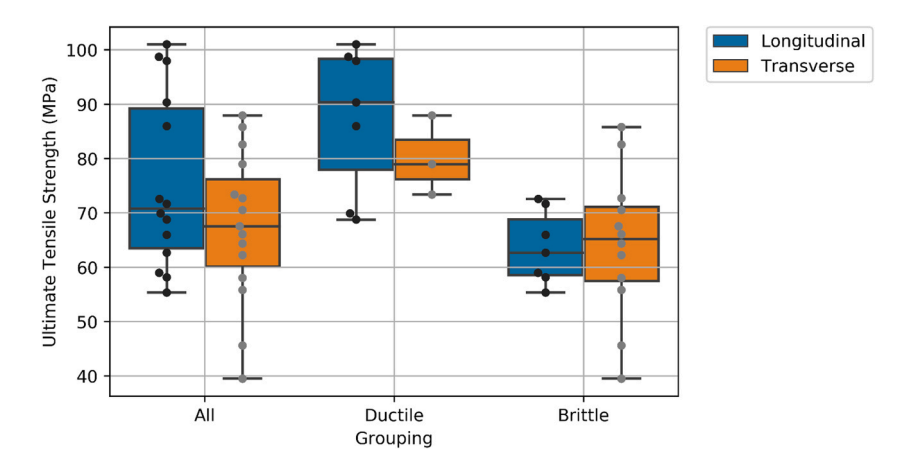


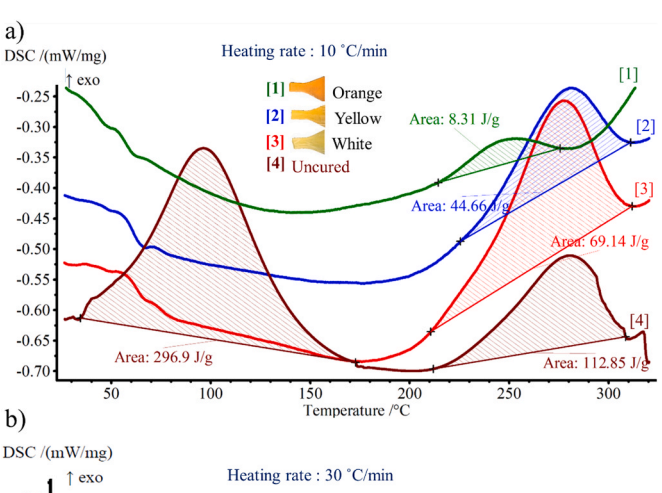
Fig. 11. Ultimate tensile strength of all specimens organized by fracture type and layer orientation.

respectively. A t-test of the transverse and longitudinal ductile tensile strengths suggested no statistically significant difference between the two (p = 0.40). While no evidence exists to suggest these two data sets come from different distributions, the limited size of the data sets makes it difficult to generalize these conclusions.

Notable color differences were present within the wall structures from which the tensile specimens were cut. The colors appear to correspond to peak cure temperatures with regions exposed to higher peak temperatures during curing becoming darker and more orange. The most orange regions of the wall structures were located in the center, which experienced the highest peak temperatures (Figs. 6, S1). Fig. 8, which depicts all specimens tested, illustrates the variation in color between specimens cut from different sections of the wall structure. Specimen color is indicative of the degree of cure within the epoxy. After gelation, the epoxy cures rapidly as long as the material remains above the glass transition temperature such that polymer chains can move within the bulk material [31]. At temperatures below the glass transition temperature, the cure rate drops due to vitrification of the material [32,33]. Accordingly, higher sustained cure temperatures can lead to more complete curing (and darkening) of the material and a tougher, more densely crosslinked polymeric material structure [34]. Qualitative inspection of the specimens led to their separation into three distinct color categories: white, yellow, and orange; these categories are utilized to investigate the relationship between ultimate strength and specimen color.

Differential scanning calorimetry (DSC) experiments were conducted on specimens from different color categories to investigate their degree of curing. Fig. 12a shows the DSC results for white, yellow, and orange specimens along with the resin/catalyst mixture. A two stage curing reaction was observed for the uncured resin/catalyst mixture. The first exothermic peak from the resin-catalyst reaction was observed at approximately 100 °C. The second exothermic peak, at approximately 280 °C, was initiated thermally at a higher temperature range, similar to that of the REAM specimens. Partially cured specimens from different color categories yielded energy peaks of dissimilar sizes and temperature ranges, ranging from approximately 210 $^{\circ}\text{C}$ to 320 $^{\circ}\text{C}$ (corresponding to approximately 20–30 min of heating at a rate of 10 $^{\circ}\text{C/}$ min), signifying differences in their degrees of curing. Integration of the exothermic peaks for different specimens showed that the degree of curing for orange, yellow, and white specimens was 98%, 91% and 86%, respectively.

Assuming the DSC results can be generalized to other specimens of the same color, the relationship between a specimen's degree of curing and ultimate tensile strength can be characterized, as shown in Fig. 13. While some uncertainty is induced by assigning curing percentages to specimens that have not been DSC tested, Fig. 13 still displays a strong linear relationship between the ultimate tensile strength of ductile



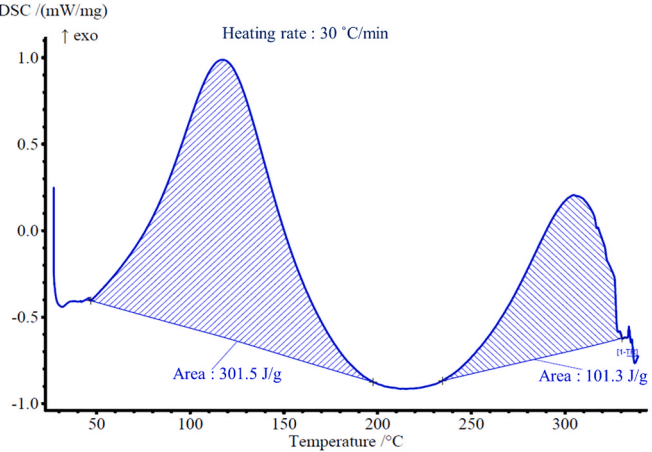


Fig. 12. (a) Dynamic DSC curves showing the enthalpy change of the partially cured specimens and the resin/catalyst mixture heated at a rate of 10 $^{\circ}$ C/min. (b) DSC curve showing enthalpy change of the resin/catalyst mixture heated at a rate of 30 $^{\circ}$ C/min. (For interpretation of the references to color in this figure legend, the reader is referred to the web version of this article.)

specimens and the specimen's degree of curing as indicated by the linear fit's r^2 value of 0.91. The mean tensile strengths of the ductile-white, ductile-yellow, and ductile-orange specimens are 72.8 ± 4.6 , 88.1 ± 2.2 MPa, and 99.2 ± 1.5 MPa respectively. T-testing performed on all three pairs of color groupings showed statistically significant differences for all comparisons ($p_{white-yellow} = 0.0033$, $p_{yellow-orange} = 0.0020$, $p_{white-orange} = 0.00023$). Moreover, the variability in ultimate tensile strength of ductile specimens is reduced from approximately ± 15 MPa (Fig. 11) to about ± 5 MPa (Fig. 13) when the degree of

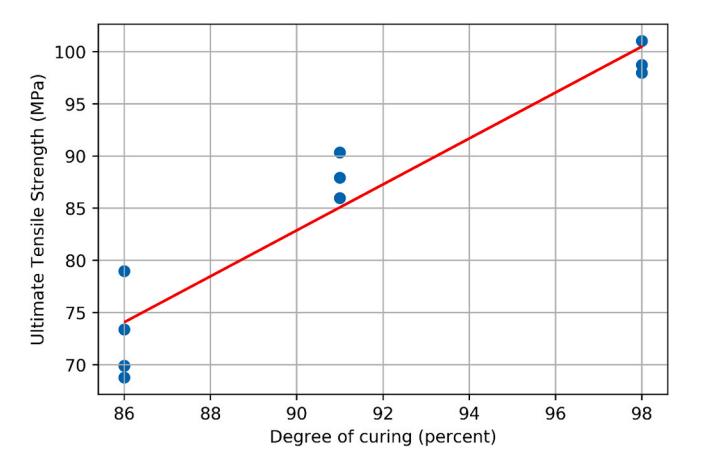


Fig. 13. Ultimate strength of ductile specimens plotted against the specimen's degree of curing with linear trendline.

curing is taken into account, suggesting that the degree of curing is responsible for most of the variability in ultimate tensile strength observed in Fig. 11.

Comparing the DSC curve for the resin/catalyst mixture (Fig. 12) with the thermal images captured at different time periods (Fig. 6) also reveals important information about the cure kinetics of the REAM parts. Thermal images suggest the part reaches an average temperature of 200 °C in 4-5 min. Analyzing the area under the DSC curve (conducted at a 30 °C/min heating rate) for the resin/catalyst mixture reveals that the resin is $\sim 75\%$ cured by the time it reaches 200 °C. The DSC results suggest that the epoxy experiences a large degree of curing in the first 4–5 min after deposition. This rapid curing enables printing of tall and uniform structures, such as the one shown in Fig. 3. The viscosity of the printed material used in this study is on the order of 10 Pa s as it enters the nozzle, which is 3–4 orders of magnitude smaller than the viscosity of inks required for direct-write AM (2, 3, 5, 15). Therefore, the evidence suggests that the degree of cure within the first few minutes of the REAM's resin/catalyst deposition is such that it enhances the viscosity by at least three orders of magnitude. The increased viscosity of the deposited material enables deposition of successive layers without distorting the preceding ones.

The elongation at break for all specimens is plotted in Fig. 14. The mean elongation at break was found to be 3.6 \pm 2.5%. A *t*-test led to acceptance of the null hypotheses that there is no statistically significant difference between the collected elongation at break data and the published value of 3.4% (p = 0.62). Extreme variation is observed in the elongation at break data, such that the median of the data, 2.3%, is smaller than the standard deviation. As shown in Figs. 9 and 14,

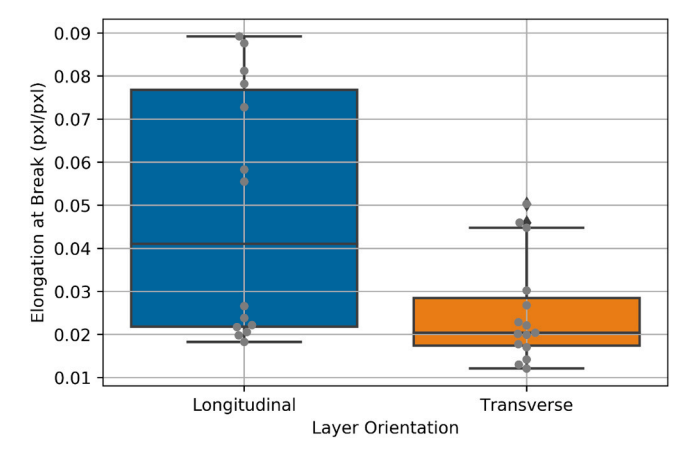


Fig. 14. Elongation at break of all specimens separated by layer orientation.

longitudinal specimens appear more likely to achieve large elongations before fracture. While only one transverse specimen managed to reach an elongation of 5% before fracturing, seven longitudinal specimens achieved the same level and more than half exceeded an elongation of 7.5%. A Welch's t-test rejected the null hypothesis that no statistically significant difference exists between transverse and longitudinal elongation at break (p = 0.0132), indicating that some of the variability in the combined data set is attributable to layer effects. It can be surmised that either brittle boundaries exist between part layers as a result of the unsynchronized cure profiles of the various layers, or that imperfections are more likely to occur between layers than within them. Of the properties evaluated thus far, elongation at break is the only property for which transverse and longitudinal specimens differ to a statistically significant degree.

Toughness data was collected for all specimens by integrating their stress-strain curves. This data is plotted for all specimens in Fig. S2. The average value and standard deviation of the toughness data for all specimens are 2.02 and 2.03 MJ/m³ respectively, indicating a high degree of variability within the data. Given toughness's dependence on the elongation at break and ultimate strength, as well as the variability of these two data sets, the large standard deviation of the toughness data relative to the mean toughness is to be expected. The mean toughness values of longitudinal and transverse specimens are 2.97 \pm 2.47 MJ/m³ and $1.12 \pm 0.88~\text{MJ/m}^3$ respectively. The former matches closely to the value of 3.052 MJ/m³ reported by Rios et al. [7] for their material formulation. Though less tough, the transverse specimens perform on par with additively manufactured nylon parts (toughness of 0.524 MJ/m³), and all tested specimens performed better than additively manufactured ABS parts (toughness of 0.152 MJ/m³) [7]. A Mann-Whitney rank test was conducted for transverse and longitudinal toughness and indicated layer orientation has a statistically significant effect on toughness (p = 0.0235).

The fracture surfaces were examined via optical microscopy (Fig. 15a) and SEM (Fig. 15b) to search for evidence of defects, such as gaseous inclusions or agglomeration of fumed silica that could adversely affect the toughness of the fabricated specimens. Optical imaging of specimen fracture surfaces showed no obvious defects or cavities, indicating that the gauge lengths of the specimens were free of gaseous inclusions. Similarly, SEM imaging showed the fumed silica to be well dispersed throughout the specimens, indicating homogeneous mixing of the fumed silica within the resin and hardener.

Based on the statistical analysis of the data collected for all 29 specimens, the only mechanical properties for which there is statistically significant evidence of layer orientation dependency are elongation at break and, consequentially, toughness. Analysis of tensile modulus and ultimate strength data suggests that, for quasi-static mechanical behavior, REAM parts are isotropic. While this isotropy does not hold for elongation at break and toughness, it represents an improvement to the anisotropy typically seen in additively manufactured parts. Moreover, the REAM process does not consistently produce parts with lower tensile strengths than that of the bulk material used in this work. Within this study, ductile parts almost universally exceeded the published cured strength of the resin used. Even amongst brittle parts, tensile strengths are on average only about 7.5% lower than the published tensile strength.

5. Comparison to other AM processes

The observed isotropy of REAM parts and their high strengths relative to published build material values compare favorably to parts manufactured using the FFF process. In FFF systems, which operate by depositing molten thermoplastic that solidifies *in situ* in a manner similar to REAM, the longitudinal strength of ABS parts can differ from their transverse strength by as much 20–42% [10,11]. The longitudinal strength of these parts, a measure of peak part strength, has been found to be as little as 75% of the strength of bulk ABS [10,11]. Both the

Fig. 15. (a) Optical microscope image of a tensile specimen fracture surface, and (b) SEM image of a tensile specimen fracture surface.

average strength and tensile modulus of the epoxy formulation reported in this paper are superior to those of thermoplastic FFF parts fabricated with ABS, PLA, Nylon, ULTEM, or carbon fiber reinforced PEKK [21,35,36]. While the longitudinal ultimate tensile strength of FFF PEEK parts have been reported by Rahman et al. [37] to be in excess of 74 MPa, they also reported considerable part anisotropy and transverse strengths between 50 and 58 MPa. Additionally, the tensile modulus of PEEK parts is lower than that of the REAM parts presented herein while achieving comparable elongations at break [37].

Anisotropy is not limited to the FFF process. Analysis of SLA parts created with an epoxy resin typically used in stereolithography found appreciable anisotropy [12], although it is not as extreme as the anisotropy seen in parts created using processes such as FFF or FGF (fused granular/granulate fabrication). The elastic modulus, Poisson's ratio, and ultimate strength of the tested SLA tensile specimens all varied by approximately 10% for different layer orientations [12]. Percent elongation at break demonstrated more significant anisotropy, in which variations as high as an order of magnitude were recorded between different layer orientations. The mechanical properties of the SLA epoxy parts [12] (with the exception of elongation at break values) match closely with those recorded for REAM specimens in this paper. This result is unsurprising because both the REAM and SLA specimens were manufactured using epoxy resin.

The build rate of the desktop system utilized in this study is fast compared to other additive manufacturing technologies. The volumetric deposition rate of the desktop REAM system is more than 20 times that of the desktop FastFFF system developed by Jamison Go and A. John Hart of MIT [29]. This comparison is particularly noteworthy given that the FastFFF system achieves flow rates more than an order of magnitude greater than commercial desktop FFF systems [29]. The 102 mL/min deposition rate of the desktop reactive extrusion system is even comparable to some large-scale, high-throughput additive systems. The BigRep Pro, an FFF system, is capable of a maximum mass deposition rate of 230 g/h [38]. Assuming a relatively low-density ABS stock is used, this corresponds to a volumetric deposition rate of 3.69 mL/min. Large scale FGF systems, while capable of much greater material throughput than typical FFF printers, are still limited by material processing constraints. THE BOX Large, one such FGF system from BLB Industries, is capable of depositing material at a rate of 30 kg/h in part by utilizing an atypically large nozzle of diameter 14 mm [39]. By again assuming compatible low-density ABS is used, the highest achievable volumetric deposition rate is 480 mL/min. The BAAM system from CINCINNATI, a particularly large thermoplastic additive system, is capable of depositing 80 lbs/h or 36.3 kg/h [40]. When using low-density ABS, this translates to a volumetric deposition rate of 672 mL/min, almost 7 times the flowrate employed in this study. While large build rates are indeed achievable by thermoplastic systems, they exacerbate the shortcomings of such systems. Large, high-energy-use heating subsystems are needed to melt the thermoplastic quickly enough. Large build rates also require specialized material, such as the carbon fiber reinforced feedstock utilized by the BAAM, to counteract

warping induced by large thermal gradients within parts during the manufacturing process.

The Reactive Additive Manufacturing (RAM) system from Magnum Venus Products is a commercially available large-scale reactive extrusion additive manufacturing system with peak deposition rate of 60 lbs/h or 27.2 kg/h [41]. Were a RAM system to use the two-part material formulation presented in this study (mixed density of 1.12 g/mL) [24, 42], its maximum volumetric flow rate would be 406 mL/min.

Recent work from de Beer et al. [19] has produced substantial improvements in SLA build speeds, achieving vertical build rates as high as 2 m per hour (two orders of magnitude faster than typical SLA machines). Assuming a build area identical to that of the desktop reactive extrusion system (0.28 m by 0.28 m), a vertical build rate of 2 m per hour, and the creation of a solid block of material utilizing the entire build area, the volumetric build rate achieved is 0.1568 cubic meters per hour or 2610 mL/min. However, very few additively created parts are so bulky or densely filled. A more realistic assumption of 20% build volume utilization yields a volumetric build rate of 0.03136 cubic meters per hour or 523 mL/min.

While the volumetric flow rate of the desktop REAM system is 4–7 times smaller than the rates of high throughput systems like the Magnum Venus RAM and CINCINNATI BAAM, the speed of the desktop REAM system is impressive when compared to the build envelope volume of the system. The volumetric flow rates, build envelope volumes, and the ratios of these values are graphed in Fig. 16 for a number of AM systems. Inspection of Fig. 16 confirms the superiority of the desktop REAM system in terms of the ratio between flowrate and build volume, i.e. the speed with which the system builds a part relative to the system's size. By virtue of the ease with which resinous materials may be transported, REAM systems are capable of rapid build rates relative to their size, rivaling industrial sized AM systems.

Because of the exotherm associated with polymerization of fast-setting thermosets, reactive extrusion AM parts require a cool-down period before they can be removed from the build plate. While the extent of this waiting period is dependent on the volume of the part and its geometry, parts such as those in Figs. 6 and 7 are typically cool enough to handle after approximately 30 min. While this post-print waiting time is longer than those associated with most desktop FFF systems, it is significantly shorter than that of typical direct-write processes, which post-cure for as long as 24 h or more [6]. Furthermore, direct-write post-print-curing typically takes place in an oven or UV chamber, limiting the size of the parts and increasing the expense and energy consumption of the entire process.

6. Conclusions

By pairing the gantry and control systems of a desktop FFF printer with a metering system, strong elastically-isotropic REAM parts can be manufactured in a fraction of the time it takes conventional polymer AM systems. These parts outperform ABS, PLA, nylon, and ULTEM parts in terms of tensile strength and stiffness while avoiding the need to expend

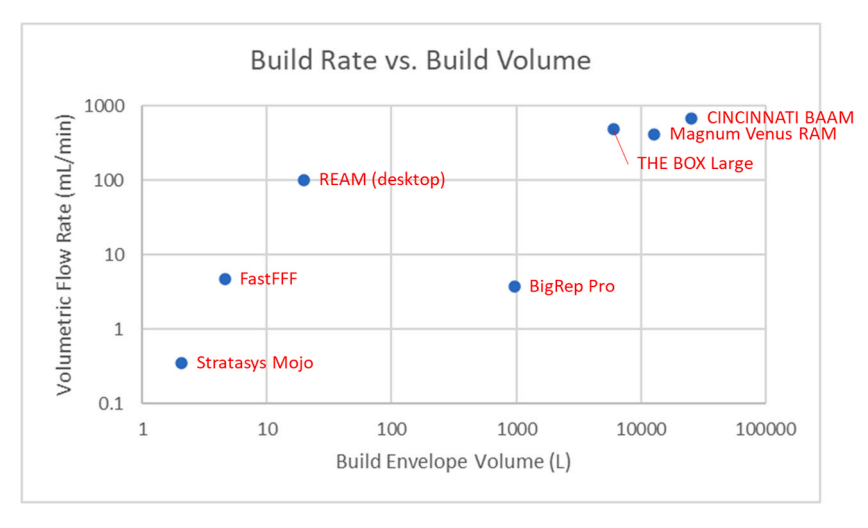


Fig. 16. Volumetric flow rate vs. build envelope volume for various AM systems [29,38-41,43].

energy on material processing during printing, as well as the need to postprocess parts to combat anisotropy [9–11,35,36]. Although FFF PEEK parts with favorable raster orientations have demonstrated longitudinal tensile strengths 4.5% larger than the average tensile strength of the REAM parts discussed herein, they are appreciably weaker in the transverse orientation, exhibiting tensile strengths between 19% and 29% lower than EPON 8111 REAM parts [37]. While printing of thermoset material is well documented in the context of direct-write systems, REAM allows one to create parts with the same class of material without post-print curing. With desktop-scale volumetric deposition rates rivaling some large-scale additive manufacturing systems, REAM presents an opportunity to create a new class of large-scale AM systems with unrivaled deposition rates.

Further development of this technology will include a focus on REAM of composite materials [44]. By leveraging existing research in direct-write thermoset composites, experimental material formulations have the potential of boosting part properties (particularly strength) by as much as an order of magnitude and mitigating the adverse effects of thermal gradients that form during in situ part curing. A second, large-scale testbed will also be developed. For example, a Yaskawa Motoman MH80 robotic arm can be combined with two progressive cavity pumps capable of generating flow rates of 800 mL/min and 200 mL/min, respectively. Such a system would be capable of pumping a two-part 4:1 ratio thermoset at a maximum rate of 1000 mL/min. Assuming no change to nozzle geometry or layer height, the hypothetical system must be able to move the nozzle at a rate of 1.08 m/s, an achievable feat for the MH80 robotic arm [45]. Such a hypothetical REAM system would therefore provide a volumetric build rate nearly an order of magnitude larger than that of the desktop system described herein.

In addition to high-throughput operation of REAM systems for the rapid fabrication of low-resolution large-scale parts, there is interest in increasing the process resolution for the purpose of creating smaller parts with fine features. The set of REAM process parameters employed in this study is notable for including an appreciably larger nozzle diameter and layer height than is typical for desktop extrusion-based AM systems. For a known flow rate and internal nozzle geometry that produces adequate precursor mixing, a decrease in nozzle diameter and/or layer height may be accompanied by an increase in nozzle speed during deposition to produce higher resolution parts. If limitations on the maximum nozzle speed constrain the process and necessitate a lower flowrate, mixing nozzles of different geometries may be tested to evaluate their ability to homogeneously mix the precursor materials at lower flowrates. By using a nozzle with a lower flowrate cutoff for adequate mixing, the nozzle diameter and/or layer height may be further reduced

for a given nozzle speed, yielding an increase in process resolution. If adequate mixing cannot be achieved at lower flowrates, an active mixing system may be used in lieu of a passive mixing nozzle.

CRediT authorship contribution statement

Oliver Uitz: Conceptualization, Methodology, Formal analysis, Investigation, Writing - original draft, Writing - review & editing. Pratik Koirala: Conceptualization, Methodology, Formal analysis, Investigation, Writing - original draft, Writing - review & editing. Mehran Tehrani: Supervision, Conceptualization, Methodology, Writing - original draft, Writing - review & editing. Carolyn Seepersad: Supervision, Conceptualization, Methodology, Writing - review & editing, Project administration, Funding acquisition.

Declaration of Competing Interest

The authors declare that they have no known competing financial interests or personal relationships that could have appeared to influence the work reported in this paper.

Acknowledgements

The authors are grateful to August Bosse, Ademola Oridate, Dr. Patricia Clayton, Dr. Mitchell Pryor, Dr. David Bourell, Dr. William O'Brien, and Dr. Zachariah Page for their contributions and insights. OU and CCS acknowledge support from the Exxon Mobil Corporation and the National Science Foundation (CMMI # 1953259). MT acknowledges support from the Office of Naval Research (ONR), under grant # N00014-20-1-2683, and the Air Force Office of Scientific Research (AFOSR), under award grant # FA9550-21-1-0066.

Appendix A. Supporting information

Supplementary data associated with this article can be found in the online version at doi:10.1016/j.addma.2021.101919.

References

- [1] J. Lindahl, A. Hassen, S. Romberg, B. Hedger, P. Hedger Jr., M. Walch, T. DeLuca, W. Morrison, P. Kim, A. Roschli, D. Nuttall, J. Czachowski, B. Post, L. Love, V. Kunc, Large-scale Additive Manufacturing with Reactive Polymers, Oak Ridge National Lab. (ORNL), Oak Ridge, TN (United States), 2018.
- [2] B.G. Compton, J.A. Lewis, 3D-printing of lightweight cellular composites, Adv. Mater. 26 (34) (2014) 59.0–5935.

- [3] N. Nawafleh, E. Celik, Additive manufacturing of short fiber reinforced thermoset composites with unprecedented mechanical performance, Addit. Manuf. 33 (2020), 101109
- [4] M.G. Odom, C.B. Sweeney, D. Parviz, L.P. Sill, M.A. Saed, M.J. Green, Rapid curing and additive manufacturing of thermoset systems using scanning microwave heating of carbon nanotube/epoxy composites, Carbon 120 (2017) 447–453.
- [5] K. Chen, X. Kuang, V. Li, G. Kang, H.J. Qi, Fabrication of tough epoxy with shape memory effects by UV-assisted direct-ink write printing, Soft Matter 14 (10) (2018) 1879–1886
- [6] N.S. Hmeidat, J.W. Kemp, B.G. Compton, High-strength epoxy nanocomposites for 3D printing, Compos. Sci. Technol. 160 (2018) 9–20.
- [7] O. Rios, W. Carter, B. Post, P. Lloyd, D. Fenn, C. Kutchko, R. Rock, K. Olson, B. Compton, 3D printing via ambient reactive extrusion, Mater. Today Commun. 15 (2018) 333–336.
- [8] S. Romberg, C. Hershey, J. Lindahl, W. Carter, B. Compton, V. Kunc, Large-scale Additive Manufacturing of Highly Exothermic Reactive Polymer Systems, Oak Ridge National Lab. (ORNL), Oak Ridge, TN (United States), 2019.
- [9] T. Letcher, M. Waytashek, Material property testing of 3D-printed specimen in PLA on an entry-level 3D printer, V02AT02A014, in: ASME International Mechanical Engineering Congress and Exposition, vol. 46438, American Society of Mechanical Engineers, 2014.
- [10] B. Rankouhi, S. Javadpour, F. Delfanian, T. Letcher, Failure analysis and mechanical characterization of 3D printed ABS with respect to layer thickness and orientation, J. Fail. Anal. Prev. 16 (3) (2016) 467–481.
- [11] S.H. Ahn, M. Montero, D. Odell, S. Roundy, P.K. Wright, Anisotropic material properties of fused deposition modeling ABS, Rapid Prototyp. J. 8 (4) (2002) 248–257
- [12] J.M. Dulieu-Barton, M.C. Fulton, Mechanical properties of a typical stereolithography resin, Strain 36 (2) (2000) 81–87.
- [13] U. Ajoku, N. Saleh, N. Hopkinson, R. Hague, P. Erasenthiran, Investigating mechanical anisotropy and end-of-vector effect in laser-sintered nylon parts, Proc. Inst. Mech. Eng. Part B J. Eng. Manuf. 220 (7) (2006) 1077–1086.
- [14] P. Calvert, T.L. Lin, H. Martin, Extrusion freeform fabrication of chopped-fibre reinforced composites, High Perform. Polym. 9 (4) (1997) 449–456.
- [15] I. Gibson, A. Mateus, P. Bartolo, RapidPRE: a new additive manufacturing technique based on reaction injection moulding, Ann. DAAAM 2010 Proc. 21 (1) (2010) 1589–1590.
- [16] I.D. Robertson, M. Yourdkhani, P.J. Centellas, J.E. Aw, D.G. Ivanoff, E. Goli, E. M. Lloyd, L.M. Dean, N.R. Sottos, P.H. Geubelle, J.S. Moore, S.R. White, Rapid energy-efficient manufacturing of polymers and composites via frontal polymerization. Nature 557 (7704) (2018) 223–227.
- [17] I.D. Robertson, E.L. Pruitt, J.S. Moore, Frontal ring-opening metathesis polymerization of exo-dicyclopentadiene for low catalyst loadings, ACS Macro Lett. 5 (5) (2016) 593–596.
- [18] M. Baumers, C. Tuck, P. Dickens, R. Hague, How can material jetting systems be upgraded for more efficient multi-material additive manufacturing, in: Proceedings of the Solid Freeform Fabrication (SFF) Symposium, The University of Texas at Austin. Texas. 2014. August.
- [19] M.P. De Beer, H.L. Van Der Laan, M.A. Cole, R.J. Whelan, M.A. Burns, T.F. Scott, Rapid, continuous additive manufacturing by volumetric polymerization inhibition patterning, Sci. Adv. 5 (1) (2019) eaau8723.
- [20] K. Yang, J.C. Grant, P. Lamey, A. Joshi-Imre, B.R. Lund, R.A. Smaldone, W. Voit, Diels-Alder reversible thermoset 3D printing: isotropic thermoset polymers via fused filament fabrication, Adv. Funct. Mater. 27 (24) (2017), 1700318.
- [21] N. Heathman, T. Yap, M. Tehrani, Hot isostatic pressing to enhance inter-laminar tensile strength of additively manufactured carbon fiber-PEKK parts, in: Proceedings of the 35th Annual American Society for Composites Technical Conference, American Society for Composites, 2020.
- [22] N.P. Levenhagen, M.D. Dadmun, Reactive processing in extrusion-based 3D printing to improve isotropy and mechanical properties, Macromolecules 52 (17) (2019) 6495–6501.

- [23] A.K. Ravi, A. Deshpande, K.H. Hsu, An in-process laser localized pre-deposition heating approach to transverse bond strengthening in extrusion based polymer additive manufacturing, J. Manuf. Process. 24 (2016) 179–185.
- [24] Hexion Inc, EPON resin 8111: Technical data sheet, 2001. (https://www.hexion.com/en-US/chemistry/epoxy-resins-curing-agents-modifiers/epoxy-tds).
- [25] B.A. Bendtsen, R.L. Ethington, Mechanical properties of 23 species of eastern hardwoods, 1975. Res. Note FPL-RN-0230. US Department of Agriculture, Forest Service, Forest Products Laboratory, Madison, WI.
- [26] D. Horvath, FW: Data for E8111+EK3271 cured/The University of Texas/ K7E3146213 [E-mail to the author], 2020, July 21. Hexion Inc. Technical Support.
- [27] P. Koirala, O. Uitz, M. Tehrani, Printability of highly viscous composite slurries via reactive extrusion additive manufacturing, in: Proceedings of the 35th Annual American Society for Composites Technical Conference, American Society for Composites, 2020.
- [28] D.R. Fenn, K.G. Olson, R.M. Rock, C. Kutchko, S.F. Donaldson, H. Sun, O. Rios, W. G. Carter, U.S. Patent Application No. 15/528,443, 2017.
- [29] J. Go, A.J. Hart, Fast desktop-scale extrusion additive manufacturing, Addit. Manuf. 18 (2017) 276–284.
- [30] A. Allan, DIC System Build to Test Additively Manufactured Parts (Master's thesis), The University of Texas at Austin, Austin, Texas, 2020.
- [31] J. Lange, N. Altmann, C.T. Kelly, P.J. Halley, Understanding vitrification during cure of epoxy resins using dynamic scanning calorimetry and rheological techniques, Polymer 41 (15) (2000) 5949–5955.
- [32] J.P. Pascault, R.J.J. Williams, Glass transition temperature versus conversion relationships for thermosetting polymers, J. Polym. Sci. Part B Polym. Phys. 28 (1) (1990) 85–95
- [33] J.K. Fink, Reactive Polymers: Fundamentals and Applications: A Concise Guide to Industrial Polymers, William Andrew, 2017.
- [34] R.J.C. Carbas, L.F.M. Da Silva, E.A.S. Marques, A.M. Lopes, Effect of post-cure on the glass transition temperature and mechanical properties of epoxy adhesives, J. Adhes. Sci. Technol. 27 (23) (2013) 2542–2557.
- [35] M. Lay, N.L.N. Thajudin, Z.A.A. Hamid, A. Rusli, M.K. Abdullah, R.K. Shuib, Comparison of physical and mechanical properties of PLA, ABS and nylon 6 fabricated using fused deposition modeling and injection molding, Compos. Part B Eng. 176 (2019), 107341.
- [36] K.I. Byberg, A.W. Gebisa, H.G. Lemu, Mechanical properties of ULTEM 9085 material processed by fused deposition modeling, Polym. Test. 72 (2018) 335–347.
- [37] K.M. Rahman, T. Letcher, R. Reese, Mechanical properties of additively manufactured PEEK components using fused filament fabrication, V02AT02A009, in: ASME International Mechanical Engineering Congress and Exposition, American Society of Mechanical Engineers, 2015.
- [38] BigRep GmbH, BigRep PRO: Industrial large scale 3D printer for professional use, 2020, June 23. (https://bigrep.com/bigrep-pro/).
- [39] BLB Industries AB, THE BOX Large: Technical specifications, n.d. (https://blbindustries.se/wp-content/uploads/2019/11/techsheet BOXlarge ENG.pdf).
- [40] Cincinnati Incorporated, Additive fact sheet: BAAM, n.d. (http://wwwassets.e-ci.com/PDF/Products/Additive-Fact-Sheet.ndf).
- [41] Magnum Venus Products, RAM: Reactive additive manufacturing, n.d. (https://www.mvpind.com/wp-content/uploads/2020/04/RAM-Brochure-Web.pdf).
- [42] Hexion Inc, EPIKURE curing agent 3271: Technical data sheet, 2001. (https://www.hexion.com/en-US/chemistry/epoxy-resins-curing-agents-modifiers/epoxy-tds)
- [43] Stratasys, Ltd, Spec Sheet Mojo, 2016. (https://support.stratasys.com/sitecore/api/downloadazurefile?id= {A9FEBC1B-BF1F-4F21-9F9B-F2FF130F8C6D}.
- [44] N. Van de Werken, H. Tekinalp, P. Khanbolouki, S. Ozcan, A. Williams, M. Tehrani, Additively manufactured carbon fiber-reinforced composites: state of the art and perspective, Addit. Manuf. 31 (2020), 100962.
- [45] Yaskawa Electric Corporation, MH80 II: Specification sheet, n.d. (https://www.motoman.com/getmedia/fd9465ed-765e-4e80-98dd-536557dbb29b/MH80II.pdf.aspx)